DOI: 10.1002/ejic.200800271

# Designed Reversible Alkylamine Intercalation–Deintercalation in the Layered Perovskite-Type Oxide $KCa_2Nb_3O_{10}$

**Chuansheng Sun,[a] Peng Peng,[a] Lirong Zhu,[b] Wenjun Zheng,*[a] and Yongnan Zhao[c]**

**Keywords:** Layered perovskites / Alkylamines / Intercalation / Deintercalation / Reversible reactions

Reactions have been designed to verify the reversibility of butylamine intercalation–deintercalation in the layered perovskite-type oxide $KCa_2Nb_3O_{10}$. The reactions include ion exchange to form $HCa_2Nb_3O_{10}\cdot 1.5H_2O$, butylamine intercalation for producing $C_4H_9NH_3Ca_2Nb_3O_{10}$, transformation of $C_4H_9NH_3Ca_2Nb_3O_{10}$ into $HCONH_3Ca_2Nb_3O_{10}$ by formamide substitution and conversion of $HCONH_3Ca_2Nb_3O_{10}$ into $HCa_2Nb_3O_{10}\cdot 1.5H_2O$ again by ion exchange. The complete reaction cycles were monitored by XRD, Raman spectroscopy, thermogravimetric (TG) and elemental analysis, and the resulting information was used to propose the structure evolution and to determine the organic components of the products. The well-matched powder X-ray diffraction (XRD) patterns and Raman spectra between the initial and recovered protonated materials confirmed that they have identical structural features of a protonated triple-layered perovskite. The C, H and N elemental analysis results and TG data indicate that the regenerated layered perovskite-type oxides also have a high capacity for alkylamine intercalation.



## Introduction

Ion-exchangeable layered perovskites $M[A_{m-1}B_mO_{3m+1}]$ (Dion–Jacobson phases) and $M_2[A_{m-1}B_mO_{3m+1}]$ (Ruddlesden–Popper phases), where $m$ represents the thickness of the perovskite-like slabs and the exchangeable interlayer cations are denoted by M, consist of 2D perovskite-like slabs featured as a sliced $ABO_3$ perovskite structure in which the A-site cation is coordinated by twelve oxygen atoms and the B-site cation is located at the centre of the $BO_6$ octahedron.[1] Both of these two phases can be feasibly converted into their protonated derivatives $H[A_{m-1}B_mO_{3m+1}]$ and $H_2[A_{m-1}B_mO_{3m+1}]$ by acid treatment.[2–8] These protonated layered perovskites have attracted much attention for their photocatalytic activity,[9] ion conductivity[10] and intercalation behaviour.[1,2,5]

As is well-known, most layered compounds can be intercalated by organic cations or molecules to form intercalation compounds.[1,5,11–13] The reaction mechanisms are based on ion exchange, ion–dipole interactions, hydrogen bonding, redox reactions and acid–base reactions. With regard to the layered-perovskite intercalation reaction, *n*-alkylamines can intercalate in the interlayer spaces by means of an acid–base mechanism.[1,5] Depending on the acidity of the protons attached to the terminal oxygen atoms along the perovskite block, organic bases with a range of $pK_b$ values can intercalate into the interlayer gallery. Because the $pK_b$ values are generally around 3.4, alkylamines are preferable choices and may be readily intercalated into Dion–Jacobson phases such as $HCaLaNb_2TiO_{10}$.[14] Also, attaching a sufficient number of protons to $NbO_6$ octahedra is proposed to enhance the interlayer reactivity. As a successful example, $HLa_2Ti_2NbO_{10}$, derived from $CsLa_2Ti_2NbO_{10}$, was found to easily intercalate alkylamines.[15] Afterwards, a series of alkylamine-intercalated layered perovskite-type oxides, $C_nH_{2n+1}NH_3Sr_2Nb_3O_{10}$ ($n$ = 1–6), were prepared through a stepwise exchange process.[16] The Ruddlesden–Popper tantalates such as $H_2CaNaTa_3O_{10}$ and $H_2Ca_2Ta_2TiO_{10}$ are another family of interesting layered perovskite materials, which can also be feasibly intercalated by alkylamines.[8,17] $H_{1.8}[Sr_{0.8}Bi_{0.2}Ta_2O_7]$, converted from an Aurivillius phase of $Bi_2SrTa_2O_9$, can accommodate *n*-alkylamines ($C_mH_{2m+1}NH_2$; $m$ = 4, 8, 12, 18) to form intercalation compounds in which the surface geometry is essentially identical to those of Dion–Jacobson phases.[18] These documented results provide approaches to a variety of alkylamine-intercalated layered perovskite-type oxides with interesting structures and properties for a wide variety of applications. The intercalation processes have been extensively investigated, whereas few studies have focused on the important issue of deintercalation chemistry, i.e. the possibility of how to remove alkylamine molecules from these intercalated layered oxides and convert intercalated com-

[a] Department of Materials Chemistry, College of Chemistry, Nankai University,
Tianjin 300071, P. R. China
Fax: +86-022-23502458
E-mail: zhwj@nankai.edu.cn
[b] Key Laboratory of Functional Polymer Materials, Ministry of Education, Nankai University,
Tianjin 300071, P. R. China
[c] Institute of Nanostructured Materials, College of Materials Science and Chemical Engineering, Tianjin Polytechnic University,
Tianjin 300160, P. R. China

  

pounds into the initial layered perovskite-type oxides. With regard to the reversibility of the intercalation–deintercalation process, two advantages are of real significance in the research on layered perovskite-type oxides. The first is the richness of the properties of these oxides, which broadens the range of intercalation derivative structures. The second is to provide a new insight into the potential for some special applications such as recycling alkylamine pollutants into useable resources by means of the intercalation/deintercalation cycle of layered perovskite-type oxides. This enables the reclaiming of layered perovskite-type oxides from waste layered intercalation materials and converting them into protonated forms that have significant potential to economise energy sources and protect the environment. On the basis of this viewpoint, a recyclable reaction chain has been designed for reversible alkylamine intercalation/deintercalation in layered perovskite-type oxides.

Layered niobates $ACa_2Nb_3O_{10}$ (A = alkali metals) are a family of the $n = 3$ Dion–Jacobson (DJ) compounds with the general formula $A[A'_{n-1}B_nO_{3n+1}]$.[2,19,20] Interestingly, the coordinating geometry of the interlayer A atom is heavily size-dependent. While the large cations of Cs and Rb reside in a distorted cubic site,[20] the small Li ion prefers to fill the tetrahedral site between adjacent perovskite layers.[21] On the other hand, the K ion with a medium size generally adopts a trigonal prismatic geometry.[22] $KCa_2Nb_3O_{10}$ and $HCa_2Nb_3O_{10}\cdot 1.5H_2O$ are lamellar Dion–Jacobson compounds that consist of perovskite slabs interleaved by potassium cations and hydrated protons.[2,19,23] Their low charge density and low interlayer covalency, relative to the structurally related Ruddlesden–Popper[24] and Aurivillius[25] phases, make them readily amenable to ion-exchange, intercalation and exfoliation reactions.[26] Herein, $KCa_2Nb_3O_{10}$ was selected as the host for reversible intercalation/deintercalation of butylamine ($C_4H_9NH_2$) molecules. $C_4H_9NH_2$ was initially inserted into the interlayer gallery for synthesising the intercalation compound $C_4H_9NH_3Ca_2Nb_3O_{10}$. It was then stepwise recovered to generate the original protonated form $HCa_2Nb_3O_{10}\cdot 1.5H_2O$ by removing $C_4H_9NH_2$. The mechanism is also discussed and suggested to be effective in elucidating the deintercalation behaviours of various layered intercalation materials.

## Results and Discussion

Figure 1 shows the XRD patterns of the products obtained from each step of a complete reaction cycle. The (110) reflection at $2\theta = 32.8°$ of HCNO1 reveals the perovskite-like slab structure along the *ab* plane.[28] The presences of the (110) peak in the samples of XCNO and HCNO2 indicate that the structure of the perovskite slab is sustained after the intercalation and deintercalation reactions. The (100) reflections observed at 23.8° in the XRD patterns of XCNO and HCNO2 imply that these products possess a simple stacking sequence without displacement (e.g. a tetragonal cell with a primitive symmetrical *P*-type cell).[29] The well-matched powder XRD patterns of XCNO and KCNO also indicate that XCNO has a structure resembling KCNO and retains the tetragonal structural features of the precursor layered phases.

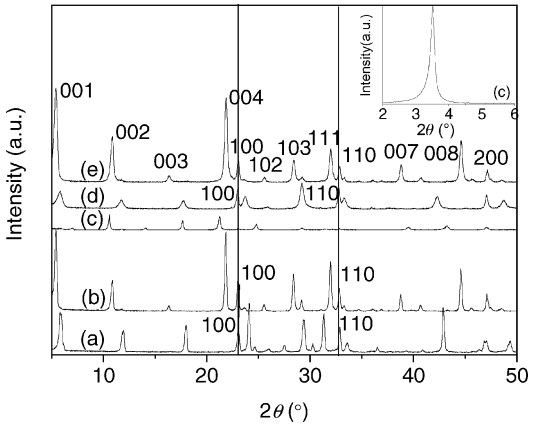


Figure 1. X-ray powder diffraction patterns of the as-synthesised samples from a complete reaction cycle: (a) KCNO, (b) HCNO1, (c) ACNO1, (d) XCNO and (e) HCNO2. The inset shows the low-angle XRD pattern of ACNO1.

A comparison between the XRD patterns of ACNO1 and ACNO2 is visible in Figure 2. The agreement between the XRD patterns of ACNO2 and ACNO1, as well as those of HCNO2 and HCNO1 (Figure 1), indicates that both the butylamine intercalated products and the protonated materials were recovered and the designed reactions for recycling the protonated phases were successful. Combining the *d* values (≈ 25.1 Å) derived from the (001) reflection peaks of ACNO1 and ACNO2, and the perovskite layer thickness (≈ 11.5 Å) of $Ca_2Nb_3O_{10}$,[3] the interlayer distance is 13.6 Å. The chain length of the butylamine is 7.6 Å. The interlayer heights of ACNO1 and ACNO2 are nearly two times the chain length of the butylamine molecule. As reported in the literature, this phenomenon can be explained by the formation of a bilayer structure of butylamine chains,[30,31] which makes the interlayer height larger than the chain length. The alkyl chains of the butylamine cations usually tilt or overlap.[32] A representative structure of the intercalated layered oxide is proposed and shown in Figure 4a.

In Figure 3, the identical powder XRD patterns between samples of XCNO and BCNO reveal that X is a formamide cation in XCNO. The component X can also be determined by the elemental analysis results and thermogravimetric analysis data. $HCONH_3Ca_2Nb_3O_{10}$ can be obtained under ultrasonic (Figure 3a, XCNO) and hydrothermal treatment (Figure 3c, B′CNO). Compared with B′CNO, sample XCNO is easier to prepare in a highly crystalline form. XCNO needs a much shorter reaction time to generate. The reason can be put down to the different reaction mechanism for producing $HCONH_3Ca_2Nb_3O_{10}$. B′CNO was produced, indicating the guest exchange process under hydrothermal conditions. However, the reaction under ultrasonic agitation occurs by an exfoliated and aggregated process. The reaction is accelerated by ultrasonic treatment. Sonication promotes the disconnection of the bilayer of bu-

  

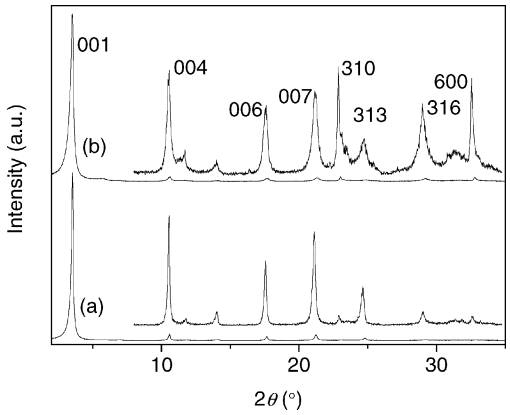


Figure 2. X-ray power diffraction patterns of the butylamine intercalated layered oxides: (a) ACNO1 and (b) ACNO2.

tylamine chains which results in rapid generation of XCNO. The exfoliated process seems comparable to that of the layered double hydroxide (LDH) which is often delaminated in formamide under ultrasonic treatment.[33] Both perovskite and LDH are ion-exchangeable layered compounds which belong to the cation-exchanged and anion-exchanged family, respectively. Because formamide is highly polar, it weakens the interlayer attraction force through the destruction of the strong hydrogen bonds between host layers and interlayer ions thereby inducing delamination.

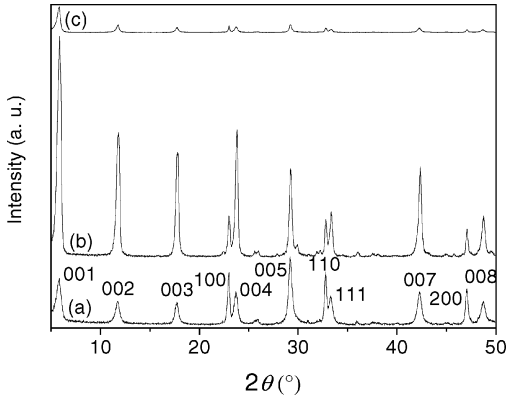


Figure 3. X-ray power diffraction patterns of the contrasting samples: (a) XCNO, (b) BCNO and (c) B′CNO.

It has been generally acknowledged that the *d* spacing ($d_{001}$) of an XCNO sample is 15.2 Å. By subtracting the thickness of the perovskite layer (≈ 11.5 Å),[3] the interlayer height of XCNO can be deduced as 3.7 Å. Since the formamide cation has a shorter chain length than butylamine and its chain length is also smaller than the unit cell of KCNO, it can lie horizontally between the two adjacent perovskite layers.[30] The H–H distance is 1.7 Å on one nitrogen atom of the formamide molecule. This result can be reasonably interpreted by the following assumption. Formamide molecules align in a protein-folding array in the interlayer gallery by means of hydrogen bonding which forms between oxygen atoms in one formamide molecule and hydrogen atoms in a neighbouring formamide molecule.[34] These H-bonded formamide chains show an unusually high degree of cooperativity. Formamide cations in the interlayer gallery are arranged as in Figure 4b.

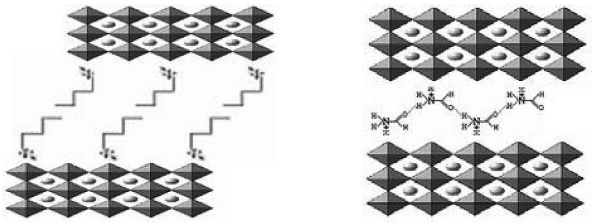


Figure 4. Two schematic structures illustrating the arrangement of interlayer cations: (a) bilayer configuration of butylamine ions in ACNO1 and ACNO2 and (b) protein-folding models of formamide ions in XCNO.

The substitution percentages of two amine-intercalated oxides can be calculated on the basis of the elemental analysis results for C, H and N which are listed in Table 1. The results give the substitution contents of 78% for ACNO1 and 71% for ACNO2. The substitution content of ACNO2 is reduced due to the decreasing granule size of the products after the deintercalation and intercalation reactions. The ultrasonic process in the reaction cycle is the main reason for the smaller granule size. As the substitution efficiency has been reported in the literature, the difficulty in reaching 100% can be reasonably interpreted by the surface geometry of the perovskite-like slab and the sizes of the *n*-alkylamines, e.g. butylamines are too bulky to fit every cavity on the surface of the perovskite-like slabs.[18] Although the fully substituted products are not available, no peaks corresponding to the precursor can be found in the XRD patterns of ACNO1 and ACNO2. This result suggests that the perovskite layers are fully propped up by butylamine in these samples. Even within the limits of experimental error, the C/N ratio (about 1:1.4) in XCNO, given by elemental analysis, further confirms that the component X in XCNO is a formamide cation. When butylamine was deintercalated from the interlayer gallery under the assistance of ultrasonic treatment, formamide substituted it to produce XCNO. The substitution percentage of XCNO can be up to 78.9%. Because of their smaller size, more formamide molecules can be intercalated into the interlayer spaces. Compared with the substitution percentage of ACNO1, the butylamine molecules in the interlayer gallery are substituted by formamide completely.

The Raman spectra of KCNO, HCNO1, ACNO1, XCNO, HCNO2 and ACNO2 are shown in Figure 5. The disappearance of the peak at 248.84 $cm^{-1}$ in HCNO1 indicates the loss of the $K^+$ ions by means of ion exchange, because the peaks in the frequency range of 100–300 $cm^{-1}$ represent the transversal vibration of $K^+$, $Nb^{5+}$ etc.[35] A blue-shift can be observed for the peak at around 574.21 $cm^{-1}$ after ion exchange. The peak at 935.71 $cm^{-1}$,

  

Table 1. Interlayer heights and elemental analysis results of the amine-intercalated layered perovskite-type oxides.

| Samples | ACNO1 | ACNO2 | XCNO |
|---|---|---|---|
| *d* value for the (001) reflection (Å) | 25.1 | 25.1 | 15.2 |
| Chain length of the intercalated amine (Å) | 7.6 | 7.6 | |
| H–H distance in one nitrogen atom (Å) | | | 1.7 |
| Interlayer height (Å) | 13.6 | 13.6 | 3.7 |
| C/N ratio | 1:3.7 | 1:3.5 | 1:1.4 |
| Substitution (%) | 78 | 71 | 78.9 |

which relates to the lattice vibration of KCNO, also undergoes a 33.58 $cm^{-1}$ blue-shift after acid exchange. These shifts reveal the strong impact of the $H^+$ which has a smaller radius and a stronger interaction with the perovskite layers than those of $K^+$.[36] The sharp peaks at 924.54 $cm^{-1}$ in ACNO1 and 925.31 $cm^{-1}$ in ACNO2 indicate that no distortion occurs in the lattice of the perovskite layers, despite the layers being propped up by the butylamine cations. This has a strong impact on the perovskite layers. These results also imply that ACNO2 retains the layered structure after a complete reaction cycle. In the reported compounds $C_nH_{2n+1}NH_3Sr_2Nb_3O_{10}$ ($n$ = 4, 5, 6), the lattice of the perovskite layers was distorted after intercalation.[16] Compared with $KSr_2Nb_3O_{10}$, the perovskite layers of $KCa_2Nb_3O_{10}$ are more stable. The A-site cation $Ca^{2+}$, having a smaller size than $Sr^{2+}$, is conducive to the stabilisation of perovskite layers. The accordance between the Raman spectra of HCNO2 and HCNO1, as well as between those of ACNO2 and ACNO1 suggests that the samples retain the layered perovskite structure after a reaction cycle. The designed reversible reactions have been successfully achieved.

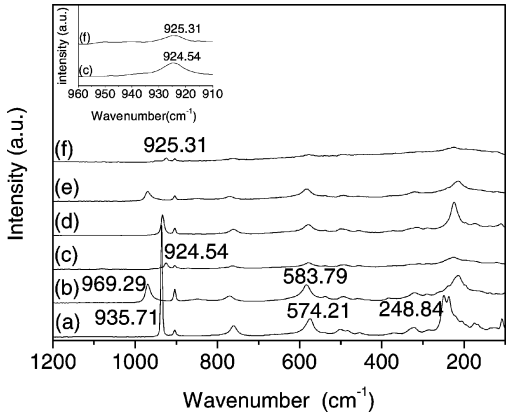


Figure 5. Raman spectra of the as-synthesised samples: (a) KCNO, (b) HCNO1, (c) ACNO1, (d) XCNO, (e) HCNO2 and (f) ACNO2. Inset shows the Raman spectra of ACNO1 around 924.54 $cm^{-1}$ and ACNO2 around 925.31 $cm^{-1}$.

Thermogravimetric analysis was performed for HCNO1, ACNO1, XCNO, HCNO2 and ACNO2 (Figure 6). The mass changes of HCNO2 agree well with those of HCNO1 and are in accordance with the corresponding weight losses for ACNO2 and ACNO1. These data confirm that HCNO2 has an identical composition to HCNO1. For HCNO1 and HCNO2, the TG curves show that the decomposition proceeds in two stages which can be ascribed to the losses of the interlayer water molecules at 60 °C and dehydroxylation at 320 °C. The mass loss for dehydroxylation is in excellent agreement with the theoretical value of 1.6 wt.-% based on the formula $HCa_2Nb_3O_{10}\cdot 1.5H_2O$. The TG curves of ACNO1 and ACNO2 exhibit gradual mass attenuation corresponding to the loss of butylamine. The guest molecule butylamine forms a bilayer structure of butylamine chains through van der Waals forces in the interlayer spaces. In general, intercalating long-chain organic bases into layered perovskites (and other layered solid acids) leads to organic/inorganic hybrid solids because the van der Waals forces that arise from the paraffin-like arrangement of the organic chains stabilise the structure.[37] When heated, butylamine molecules on the fringe of the perovskite interlayer are more easily lost and the butylamine molecules in the interlayer spaces are lost later. A slight mass gain, evident in the TG curves of ACNO1 and ACNO2 from 600 to 700 °C, originates from the absorption of $N_2$. From the TG data, the substitution content of butylamine can be estimated as 77.0% for ACNO1 and 66.6% for ACNO2. Evidently, both ACNO1 and ACNO2 have a high substitution percentage. The TG curve of XCNO shows a two-step mass loss which can be attributed to the emission of the formamide molecules at around 240 °C and dehydroxylation at around 390 °C. This decomposition process can also be verified by XRD measurements (Figure 7). The substitution content of formamide was estimated as 81.7% for XCNO. A small amount of $N_2$ absorption can also be seen at around 600 °C in the TG curve of XCNO.

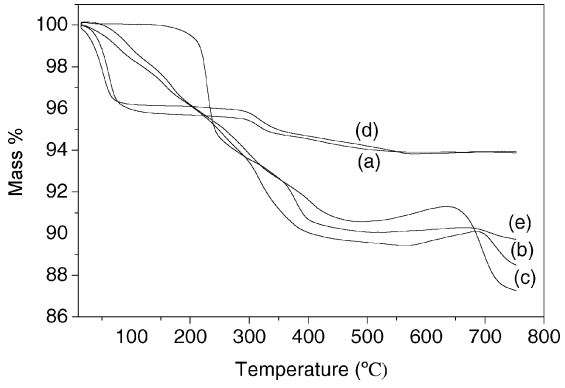


Figure 6. Thermogravimetric analysis curves of the as-synthesised samples: (a) HCNO1, (b) ACNO1, (c) XCNO, (d) HCNO2 and (e) ACNO2.

The progression of the powder X-ray diffraction patterns corresponding to the XCNO phase changes is illustrated in Figure 7. The shift of the characteristic (001) peak shows that heating XCNO at 320 °C results in the loss of formamide and dehydroxylation occurs to transform XCNO into the metastable compound $Ca_4Nb_6O_{19}$ at 500 °C.[38] The decomposition processes may be expressed by Equations (1) and (2):

  

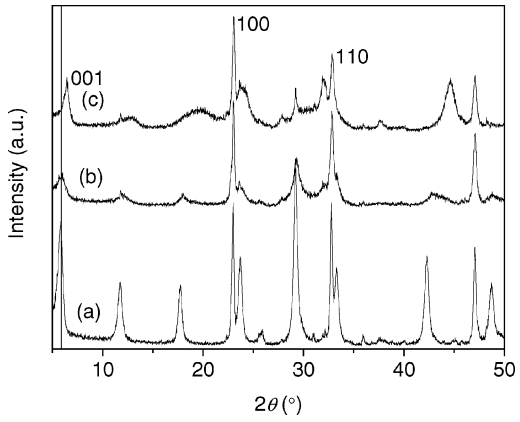


Figure 7. X-ray power diffraction patterns of (a) the as-synthesised XCNO, (b) samples annealed at 320 °C and (c) 500 °C.

$$HCONH_3Ca_2Nb_3O_{10} \rightarrow HCa_2Nb_3O_{10} + CO + NH_3 \quad (1)$$

$$2\ HCa_2Nb_3O_{10} \rightarrow Ca_4Nb_6O_{19} + H_2O \quad (2)$$

Upon heating, the characteristic (001) reflection peak shifts gradually towards a higher $2\theta$ angle, indicating that molecules evaporate from the interlayer spaces. XRD patterns of the sample reveal that the (110) reflection at $2\theta$ = 32.8° and the (100) reflection at $2\theta$ = 23.8°, characteristic of the in-plane structure, is unchanged. This indicates that the layered structure is preserved for the products.

We propose that the reversible intercalation/deintercalation reactions are governed by the acid–base type exchange reaction between butylamine and formamide in the interlayer space and the ion-exchange type reaction which recycles the protonated form of the perovskite, as schematically illustrated in Figure 8. The acid–base type reaction between ethylenediamine and exfoliated tetratitanic acid nanosheets was proposed by Sugimoto et al.[39] Reaction between one of the amine groups in ethylenediamine and the surface OH group of a tetratitanic acid nanosheet occurs first. By analogy with the reaction of ethylenediamine and exfoliated tetratitanic acid nanosheets, herein the bilayers of butylamine chains are disconnected under ultrasonic treatment in formamide solvents (Figure 8b). Butylamine is then deintercalated from the perovskite nanosheets and dissolves in the formamide solvent. The interlayer gallery swells with solvent until the forces that hold the layers together are overcome and the solid delaminates to form a colloidal suspension of sheets (Figure 8c).[17,23,40] The amine group of formamide first reacts with the accessible surface OH group of a nearby exfoliated perovskite acidic nanosheet by means of an acid–base reaction (Figure 8d). The H-bonded chains then form between formamide molecules in the interlayer spaces. The reassembly of the formamide-modified exfoliated perovskite acidic nanosheets occurs by interaction between the formamide molecules covering the surface of the exfoliated acid nanosheet (Figure 8e). Formamide molecules align in the protein-folding array in the interlayer gallery by means of hydrogen bonding. All the formamide molecules exist as a whole in the interlayer space. Compared with butylamine, formamide is more easily accommodated in the interlayer gallery under ultrasonic treatment. The H-bonded chains are completely optimised by the restraint that the formamide molecules are all geometrically equivalent and coplanar with each other.[34] When XCNO reacts with the acid solution, water molecules are adsorbed into the interlayer space. The augmentation of the interlayer heights originates from water insertion and the H-bonded chains between the formamide molecules are ruptured. Formamide molecules then depart from the nanosheets and the protonated compounds are obtained by ion exchange. According to the formula $HCa_2Nb_3O_{10}\cdot 1.5H_2O$, water molecules in the interlayer gallery may exist in the form of $H_3O^+$ and $H_5O^{2+}$ cations in a molar ratio of 1:1 (Figure 8g). The proposed reaction mechanism explains why butylamine can be replaced by formamide in the interlayer space and formamide-intercalated layered perovskite-type oxides can be converted into the protonated forms.

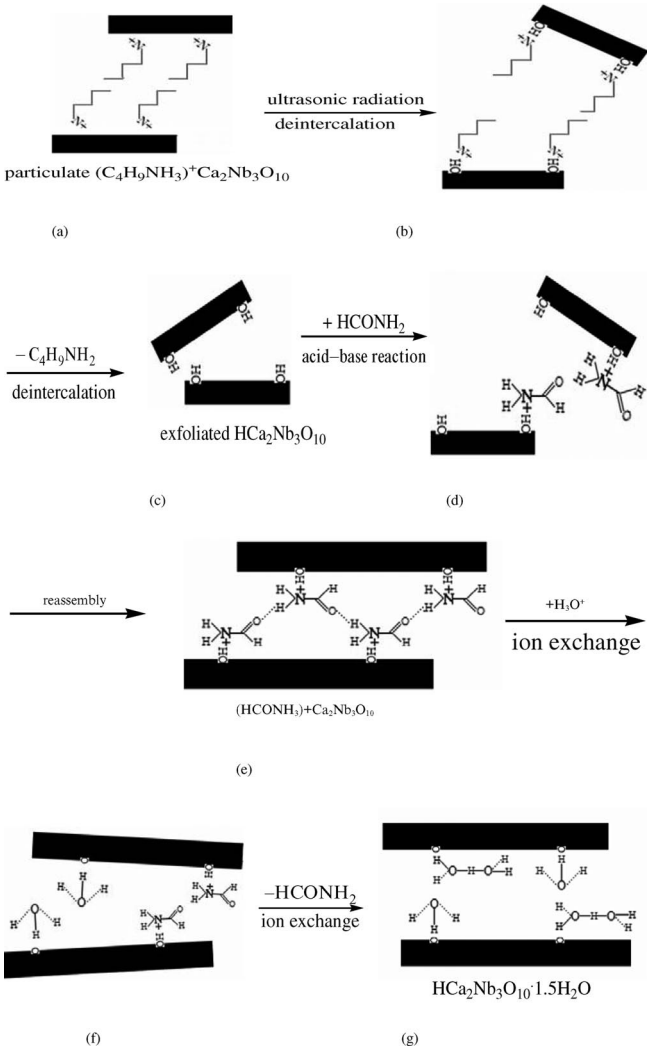


Figure 8. The proposed reaction scheme for recycling a butylamine-intercalated layered perovskite-type oxide to its protonated form.

  

## Conclusions

The complete cycle of reactions has been successfully designed to bring about the reversibility of butylamine intercalation–deintercalation in the layered perovskite oxide $KCa_2Nb_3O_{10}$. The recycling is achieved stepwise by substituting butylamine by formamide under ultrasonic agitation and then ion exchange. After recycling, the butylamine-intercalated layered perovskite-type oxide is transformed into the protonated form. The composition and structural features of the recycled protonated compounds agree with the original forms. The recycled protonated compounds also have a high percentage of substitution to accommodate butylamine. The recovery of the protonated materials with unchanged characteristics proves that our designed reactions provide an effective route for the deintercalation of alkylamines from the layered intercalated materials. Furthermore, replacing butylamine by formamide in our reaction cycle provides a new approach for exchanging different types of amines in the perovskite interlayer spaces.

## Experimental Section

The layered oxide $KCa_2Nb_3O_{10}$ (denoted as KCNO) was prepared by calcining a mixture of $K_2CO_3$, $CaCO_3$ and $Nb_2O_5$ in a stoichiometric ratio (K/Ca/Nb = 1.2:2:3) in air at 1200 °C for 20 h. An ion-exchange reaction of KCNO was carried out in $HNO_3$ solution to afford the protonated form $HCa_2Nb_3O_{10}\cdot 1.5H_2O$ (denoted as HCNO1). Treatment of the protonated form with *n*-butylamine gave $C_4H_9NH_3Ca_2Nb_3O_{10}$ (denoted as ACNO1).[27] Afterwards, ACNO1 was dispersed into formamide and the mixtures were sonicated for 0.5 h. ACNO1 was transformed into a new material (denoted as XCNO) and butylamine molecules were eliminated. XCNO was then converted into the protonated compounds $HCa_2Nb_3O_{10}\cdot 1.5H_2O$ (HCNO2) by ion exchange as mentioned above. Finally, $C_4H_9NH_3Ca_2Nb_3O_{10}$ (denoted as ACNO2) was reproduced by dispersing HCNO2 in butylamine.

To confirm that the intermediate XCNO is a formamide intercalated derivative, contrast experiments were run by soaking HCNO1 in a mixture of ethanol and formamide. The mixture was transferred into an autoclave, followed by hydrothermal treatment. $HCONH_3Ca_2Nb_3O_{10}$ (denoted as BCNO) was obtained. We also prepared $HCONH_3Ca_2Nb_3O_{10}$ (denoted as B′CNO) by soaking ACNO1 in formamide under hydrothermal conditions at 120 °C for 3 d.

Powder X-ray diffraction (XRD) patterns were measured with a Rigaku D/max 2500 V/PC diffractometer by using Cu-$K_\alpha$ radiation ($\lambda$ = 1.54056 Å, 40 kV, 100 mA). The proportion of volatile elements C, H and N were analysed by using a Vario EL3 elemental analyser. Raman spectra were recorded at room temperature with a Bruker RFS-100 spectrometer. Thermogravimetric (TG) analyses were performed with a NETZSCH TG 209 instrument at a heating rate of 10 °C min$^{-1}$ in air.

## Acknowledgments

We thank the National Natural Science Foundation of China (No. 20571044) for financial support for this work.

[1] R. E. Schaak, T. E. Mallouk, *Chem. Mater.* **2002**, *14*, 1455–1471.
[2] A. J. Jacobson, J. W. Johnson, J. T. Lewandowski, *Inorg. Chem.* **1985**, *24*, 3727–3729.
[3] A. J. Jacobson, J. T. Lewandowski, J. W. Johnson, *J. Less Common Met.* **1986**, *116*, 137–146.
[4] J. Gopalakrishnan, V. Bhat, *Inorg. Chem.* **1987**, *26*, 4299–4301.
[5] J. Gopalakrishnan, V. Bhat, B. Raveau, *Mater. Res. Bull.* **1987**, *22*, 413–417.
[6] M. Richard, L. Brohan, M. Tournoux, *J. Solid State Chem.* **1994**, *112*, 345–354.
[7] S.-H. Byeon, J.-J. Yoon, S.-O. Lee, *J. Solid State Chem.* **1996**, *127*, 119–122.
[8] R. E. Schaak, T. E. Mallouk, *J. Solid State Chem.* **2000**, *155*, 46–54.
[9] J. Yoshimura, Y. Ebina, J. Kondo, K. Domen, A. Tanaka, *J. Phys. Chem.* **1993**, *97*, 1970–1973.
[10] M. Sato, J. Abo, T. Jin, M. Ohta, *J. Alloys Compd.* **1993**, *192*, 81–83.
[11] A. J. Jacobson, "Intercalation Reactions of Layered Compounds" in *Solid State Chemistry*: *Compounds* (Eds.: A. K. Cheetham, P. Day), Clarendon Press, Oxford, **1992**, pp. 182–211.
[12] D. O'Hare, "Inorganic Intercalation Compounds" in *Inorganic Materials*, 2nd ed, (Eds: D. W. Bruce, D. O'Hare), John Wiley & Sons, Chichester, **1996**, pp. 171–188.
[13] B. K. G. Theng in *The Chemistry of Clay-Organic Reactions*, Adam Hilger, London, **1974**, pp. 243–260.
[14] J. Gopalakrishnan, S. Uma, V. Bhat, *Chem. Mater.* **1993**, *5*, 132–136.
[15] Y. S. Hong, S. J. Kim, S. J. Kim, J. H. Choy, *J. Mater. Chem.* **2000**, *10*, 1209–1214.
[16] Z. Zhong, W. Ding, W. Hou, Y. Chen, *Chem. Mater.* **2001**, *13*, 538–542.
[17] R. E. Schaak, T. E. Mallouk, *Chem. Mater.* **2000**, *12*, 3427–3434.
[18] Y. Tsunoda, W. Sugimoto, Y. Sugahara, *Chem. Mater.* **2003**, *15*, 632–635.
[19] M. Dion, M. Ganne, M. Tournoux, *Mater. Res. Bull.* **1981**, *16*, 1429–1435.
[20] a) M. Dion, M. Ganne, M. Tournoux, J. Ravez, *Rev. Chim. Miner.* **1984**, *21*, 92–103; b) M. Dion, M. Ganne, M. Tournoux, *Rev. Chim. Miner.* **1986**, *23*, 61–69.
[21] K. Toda, T. Teranishi, Z.-G. Ye, M. Sato, Y. Hinatsu, *Mater. Res. Bull.* **1999**, *34*, 971–982.
[22] H. Fukuoka, T. Isami, S. Yamanaka, *J. Solid State Chem.* **2000**, *151*, 40–45.
[23] M. M. J. Treacy, S. B. Rice, A. J. Jacobson, J. T. Lewandowski, *Chem. Mater.* **1990**, *2*, 279–286.
[24] a) S. N. Ruddlesden, P. Popper, *Acta Crystallogr.* **1957**, *10*, 538–539; S. N. Ruddlesden, P. Popper, *Acta Crystallogr.* **1958**, *11*, 54–55; b) S. Una, A. R. Raju, J. Gopalakrishnan, *J. Mater. Chem.* **1993**, *3*, 709–713.
[25] B. Aurivillius, *Ark. Kemi.* **1949**, *1*, 463–480.
[26] A. J. Jacobson, *Mater. Sci. Forum.* **1994**, *1*, 152–153.
[27] A. J. Jacobson, J. W. Johnson, J. T. Lewandowski, *Mater. Res. Bull.* **1987**, *22*, 45–51.
[28] S. Tahara, Y. Sugahara, *Langmuir* **2003**, *19*, 9473–9478.
[29] Y. Tsunoda, M. Shirata, W. Sugimoto, Z. Liu, O. Terasaki, K. Kuroda, Y. Sugahara, *Inorg. Chem.* **2001**, *40*, 5768–5771.
[30] H. Izawa, S. Kikkawa, M. Koizumi, *Polyhedron* **1983**, *2*, 741–744.
[31] C. Philippe, M. C. R. René, *Acad. Sci. Ser. II* **1983**, *296*, 1161–1165.
[32] J.-F. Lambert, Z. Deng, J.-B. D'Espinose, J. J. Fripiat, *J. Colloid Interface Sci.* **1989**, *132*, 337–351.
[33] a) Q. Wu, A. Olafsen, Ø. B. Vistad, J. Roots, P. Norby, *J. Mater. Chem.* **2005**, *15*, 4695–4700; b) R. Ma, Z. Liu, K. Takada, N. Iyi, Y. Bando, T. Sasaki, *J. Am. Chem. Soc.* **2007**, *129*, 5257–

  

5263; c) T. Hibino, *Chem. Mater.* **2004**, *16*, 5482–5488; d) M. Jobbágy, A. E. Regazzoni, *J. Colloid Interface Sci.* **2004**, *275*, 345–348; e) L. Li, R. Ma, Y. Ebina, N. Iyi, T. Sasaki, *Chem. Mater.* **2005**, *17*, 4386–4391.
[34] N. Kobko, L. Paraskevas, E. del Rio, J. J. Dannenberg, *J. Am. Chem. Soc.* **2001**, *123*, 4348–4349.
[35] N. Sidorov, M. Palatnikov, Y. Serebryakov, *Ferroelectrics.* **1996**, *188*, 31–40.
[36] Z. Zhong, W. Ding, Y. Chen, X. Chen, Y. Zhu, N. Min, *Appl. Phys. Lett.* **1999**, *75*, 1958–1960.
[37] a) G. Lagaly, *Solid State Ionics.* **1986**, *22*, 43–51; b) N. Kinomura, N. Kumada, *Solid State Ionics.* **1992**, *51*, 1–5; c) N. S. P. Bhuvanesh, J. Gopalakrishnan, *Inorg. Chem.* **1995**, *34*, 3760–3764.
[38] M. Fang, C. H. Kim, T. E. Mallouk, *Chem. Mater.* **1999**, *11*, 1519–1525.
[39] W. Sugimoto, K. Ohuchi, Y. Murakami, Y. Takasu, *Bull. Chem. Soc. Jpn.* **2005**, *78*, 633–637.
[40] a) M. Fang, H.-N. Kim, G. B. Saupe, T. Miwa, A. Fujishima, T. E. Mallouk, *Chem. Mater.* **1999**, *11*, 1526–1532; b) R. E. Schaak, T. E. Mallouk, *Chem. Mater.* **2000**, *12*, 2513–2516.

Received: March 14, 2008
Published Online: July 11, 2008

  